

How processing affects relative reflection amplitudes

David C. Henley and Joe Wong

ABSTRACT

One objective of seismic data processing is to reduce both coherent and random noise contaminating the reflection data, so that the physical properties of the rocks and their contained fluids may be more readily estimated and/or imaged from trace amplitudes. During the processing, it can be important to preserve the relative amplitudes of reflection events, especially laterally (trace-to-trace), since several interpretive techniques are based on amplitude comparisons. Most prominently, AVO and AVA methods compare amplitudes from the same reflection or conversion event at different source-receiver offsets (AVO), or at different raypath angles (AVA). We describe here an empirical study in which physical model data were subjected to three commonly used processing techniques. The amplitudes along single reflections in those data were compared at each stage of processing. We found that, within the limits of measurement error, subtractive noise attenuation (radial trace filtering) and non-stationary deconvolution (Gabor deconvolution) have no significant effect on relative event amplitudes. As we might expect, however, a multi-trace process like F-X deconvolution, does affect relative event amplitudes and should probably be avoided in processing data for AVO.

INTRODUCTION

Processing and trace amplitudes

As seismic technology has matured, it has aimed increasingly at extracting more information from seismic data than a simple reflection image. Various theoretical developments prompted interpreters to begin looking at new aspects of the data. Of considerable interest is the variation along an interface of reflectivity (or “convertivity” for 3C data) with the angle of incidence of the seismic energy. To use the new interpretive methods based on the theory, it becomes important that processing algorithms applied to the data prior to interpretation of event amplitudes not alter the relative amplitudes of the same event as expressed on different seismic traces.

Many of the algorithms developed to process seismic reflection data are aimed at producing the most interpretable structural image of a cross-section of the Earth. When imaging is the goal, and data redundancy is large, we apply various techniques that trade off redundancy for event coherence and resolution. Multi-trace filtering and smoothing, and various kinds of stacking and migration algorithms are some of the more obvious processes of this type, and they all disturb or destroy trace-to-trace amplitude variations. Furthermore, some of the single-trace processes we apply, if they attempt to scale overall trace amplitudes to a common level, also remove AVO information. These include operations like AGC or trace normalization, since these can greatly alter trace-to-trace amplitudes.

Physical modeling

One of the objectives of the new CREWES physical modeling system (Wong et al, 2007, 2008, 2009) is to study phenomena which are manifested as variations of event amplitude with incident angle, in order to compare measured results with theoretical predictions. The data created with this system suffer some of the same effects seen on seismic field data, including contamination by both coherent and random noise, and the bandlimiting effects of seismic energy transmission through physical media. In many cases, then, we need to apply some processing in order to enhance the events enough to measure them reliably. This is particularly true when the model is such that very strong source-generated noise is spread across the source gather, the vertical stack-fold is insufficient to suppress random noise, or the seismic event wavelet visibly broadens with penetration into the model. Hence, we processed a set of physical modeling data using three of our standard processing modules for coherent noise attenuation, non-stationary deconvolution, and random noise attenuation, respectively, to analyze and document any unacceptable modification of relative amplitudes along three different reflection events in the model, caused by the effects of the processing modules.

MODEL DATA SET

As described by Wong et al (2007, 2008, 2009), the physical modeling facility at CREWES is an ultrasonic transducer-based automated system intended to perform large, detailed seismic surveys of various earth models designed in the laboratory to have various elastic properties. The materials used to construct the layers of various models can include water, aluminum, plexiglass, and phenolic resin with embedded fabric layers (intended to model anisotropic materials). The data we analyzed in the current report were obtained from three separate surveys on a simple model with an anisotropic lower layer. One survey was performed in-line with the slow axis of the layer, one at right angles to the axis, and one oriented at 45 degrees to it. Each survey generated a single simulated source gather.

Although we can control the elastic properties and geometrical configuration of the model, as well as the acquisition parameters, the measured wavefield responses are vulnerable to many of the same problems encountered in the acquisition of seismic field data. Therefore, we must generally apply processing of some kind to physical model data, just as we do to seismic field data. The ideal, however, is to use the minimum amount of processing necessary to cosmetically enhance the data, without changing the attributes we seek to study. In our usage, ‘enhancement’ mainly means improving the S/N of reflection events (with respect to both random and coherent noise), while retaining the relative reflection amplitudes from trace to trace across a trace gather. We routinely use radial trace (R-T) filtering to attenuate coherent noise on trace gathers (Henley, 2003), and Gabor deconvolution to improve the bandwidth and hence the resolution of reflections (Margrave et al, 2002, 2003). Random noise is often attacked by a multi-channel technique such as F-X deconvolution, or by increasing the fold of any vertical stacking used in acquisition. Hence, we examine the effects on the amplitudes of various reflections, in the physical model, of three standard processing techniques: radial trace filtering, Gabor deconvolution, and F-X deconvolution. We do not examine the effects of such multi-trace operations as pre-stack migration or f-k filtering, since these are already

known to have effects on AVO. Although we examined three sets of physical modeling data corresponding to the three acquisition directions described above, we show here the results for only one of those data sets, since all results were similar.

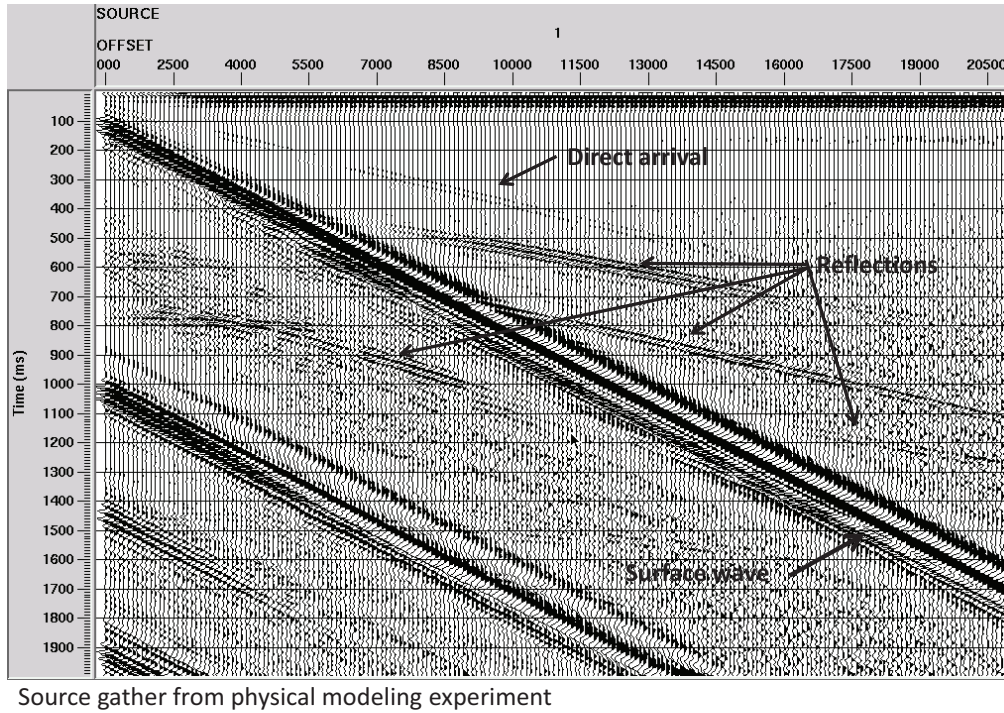


FIG. 1. Source gather from a physical modeling experiment showing the strong surface wave dominating the much weaker reflections and direct arrival. A relatively high level of random noise is also visible.

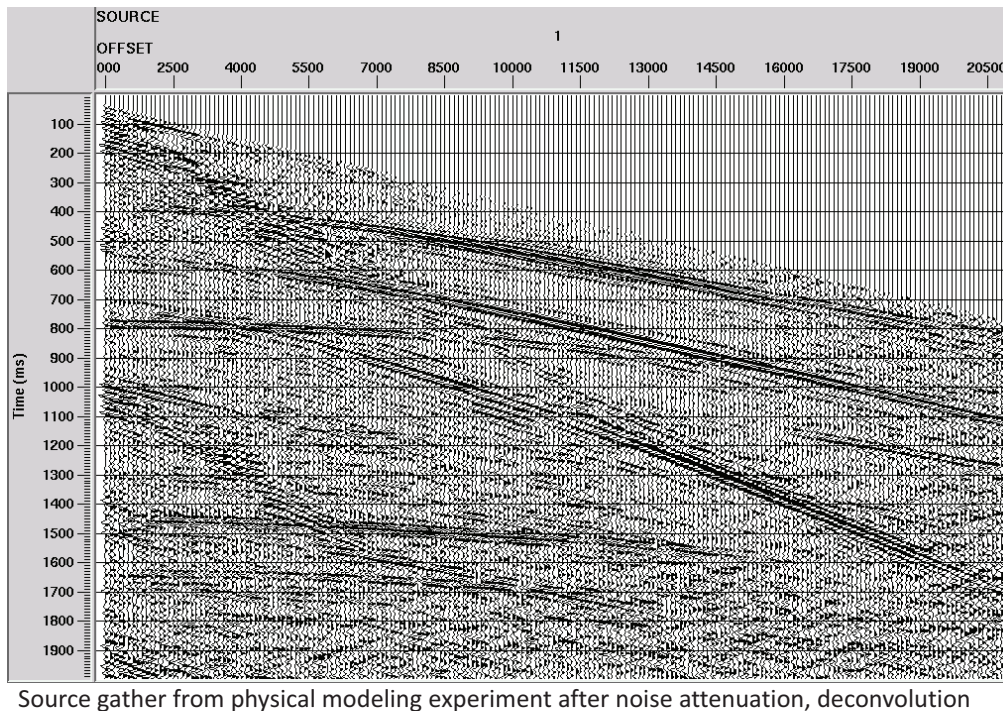


FIG. 2. Source gather from Figure 1 after coherent noise attenuation and Gabor deconvolution. Many reflection events are now visible, but are the AVO amplitude relationships intact?

Figure 1 shows a typical shot gather record from a physical modelling experiment, with only AGC applied before display. Several features of this record are immediately evident. The coherent linear noises (surface waves) are by far the strongest events on the record, and the reflections the weakest. If we had not applied AGC to this display, the reflections would not be visible at all. Also, a significant level of random noise is apparent. Finally, the waveforms of all events seem longer than the single bandlimited pulse that we prefer. Figure 2 shows the same shot after processing with R-T coherent noise attenuation, Gabor deconvolution, and F-X deconvolution (and AGC to level relative trace amplitudes for display). It is clear that the reflections are much more prominent, that their waveforms have been slightly shortened, and that their amplitudes will be correspondingly easier to measure; but are the relative amplitudes from trace to trace properly preserved (before AGC)? Below, we discuss what effect we expect intuitively from each processing operation, then we describe how we actually measure amplitudes along reflections before and after each operation, in order to detect whether the AVO relationships have changed.

Coherent noise attenuation

Many coherent noise attenuation algorithms are multi-channel operations with the potential to average amplitudes laterally, usually along dip directions corresponding to prominent noises. If the averaging is used only in the process of estimating specific coherent noises, which are subsequently subtracted from the raw data, alteration of the underlying reflection amplitudes is minimal. This type of filter includes the radial trace filter algorithm as we practice it (estimate-and-subtract). This algorithm transforms an input trace gather to the radial trace (R-T) domain, applies a low-pass filter to exclude

reflection energy and isolate the coherent linear noise, then subtracts this noise estimate from the original gather back in the X-T domain. If the noise estimate contains no reflection energy, then its subtraction from the raw data will not affect the reflection amplitudes. If, however, the low-pass filter has admitted some portion of the reflection energy, or if the noise amplitude itself is not accurately estimated, then its subtraction can alter reflection amplitudes, at least in the vicinity of the noise events. Since the radial trace filtering process typically includes several cascaded passes of the filter module, the compounded effects of the filters on reflection amplitudes should be detectable, if they are significant.

Deconvolution

Since deconvolution is normally a single-trace operation which affects only the reflection amplitudes on a single trace, we would not ordinarily expect it to affect AVO relations on a noise-free reflection event. In the presence of significant random noise, however, the S/N of a particular reflection may vary from trace to trace. This would affect the degree of whitening experienced by a particular reflection on each trace. This, in turn, would affect the ‘measurable amplitude’ of an event, since amplitudes measured from trough to peak will be different for different bandwidth manifestations of the same event. A further potential complication arises with non-stationary deconvolution, like the Gabor operation, since the reflection amplitudes in one time window have an influence on amplitudes in other time windows on the same trace, due to the smoothing applied to the Gabor spectrum. One mode of operation, however, in which we would *not* expect trace-to-trace amplitude effects is the ensemble-average mode, since a single Gabor operator is estimated from all the traces in a gather, then applied to each trace individually. Although our Gabor deconvolution algorithm normalizes the traces in each input ensemble before deconvolution, it removes the normalization factor for each trace before output.

Random noise attenuation

Most of the effective processes for attenuating random noise rely on multi-trace averaging of some sort, often along various dip directions. The F-X deconvolution operation is no exception, in that it analyzes input data in the F-X domain and attempts to ‘predict’ the meaningful events. The derived prediction filters are used to reconstruct the data, hopefully with less random noise, since this noise is minimally predictable. Intuitively, we expect this type of filter not to have a large effect on legitimate reflection amplitudes from trace to trace; but there is always the potential with prediction filters to ‘create’ events from higher amplitude random noise.

Vertical stacking

Vertical stacking refers to the practice, with weak seismic sources, of summing many successive ‘shots’ of the source in order to build up the strength of the coherent events and average out the truly ‘random’ noise in the seismic band. It is a common practice when using low-energy long-duration sources like Vibroseis, as well as low-energy highly-repeatable sources like the piezoelectric transducers in our modelling system. For the data we show here, a modest vertical stack fold was used, resulting in some residual random noise surviving on the seismic records. This random noise manifests itself as

fluctuations of amplitude measurements (“jitter”) along reflection events, increasing the ‘error bars’ of the amplitude measurements.

Amplitude measurement

There are many attributes of reflection waveforms that can be taken as measurements of the amplitude of a waveform. We choose a maximum minus minimum amplitude difference, where both the maximum and minimum are determined within a window framing the event waveform. This is a relatively robust measurement, since the minimum and maximum are relatively easy to locate unambiguously automatically. A more robust amplitude measurement might actually be a sum of the samples or squared samples of the entire waveform; but this is more difficult to do automatically, since the starting and ending points for the sums must be accurately located for each trace independently. Such an attribute would be relatively independent of event bandwidth, but the difficulty in computing it would increase with the level of noise.

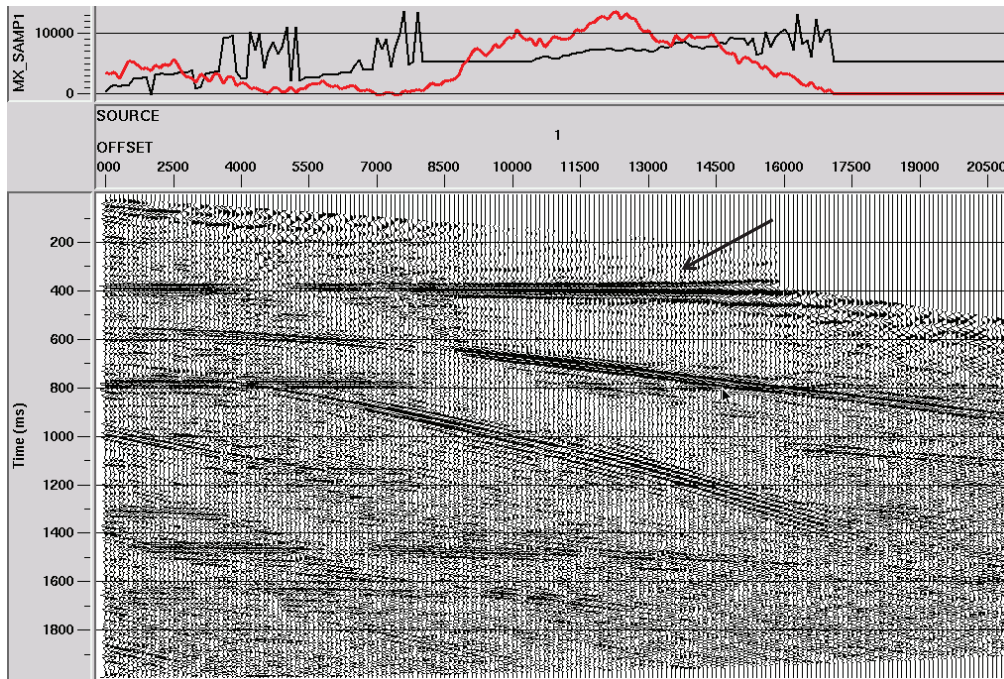
PROCEDURE

The simple analysis method we used for determining the effect of our three processing operations on physical model seismic data was to first apply the operations to be analyzed. Then we applied NMO appropriate for a targeted reflection event to the subject trace gather, a bandpass filter to attenuate high-frequency random noise (above the seismic band), followed by a ProMAX module which searched each trace within a time window for the absolute minimum and the absolute maximum of the waveform within the window. The trough-to-peak (maximum minus minimum) amplitudes were posted to special trace headers, as were the nominal time picks of the maxima, in order to plot them on the trace displays of the events. Because the reflection events had been flattened by NMO, the amplitude module had little difficulty picking the reflection amplitudes, except where these amplitudes were overwhelmed by noise. The application of NMO correction has no effect on event amplitudes, since the trace samples are carefully interpolated during the stretching process. Likewise, the bandpass has no net amplitude effect, since the filter is properly normalized. In any case, since the same NMO correction and bandpass are applied in every analysis, any effects would cancel when comparing the analyses with each other. We used our analysis method on three reflection events on the subject shot record, after each stage of processing. After all the analyses, we created an amplitude overlay plot on which we can assess the relative effects of each stage of processing. In every case, although reflection amplitudes were measured on un-normalized traces, whole-trace normalization was applied to traces before display to improve visibility.

RESULTS

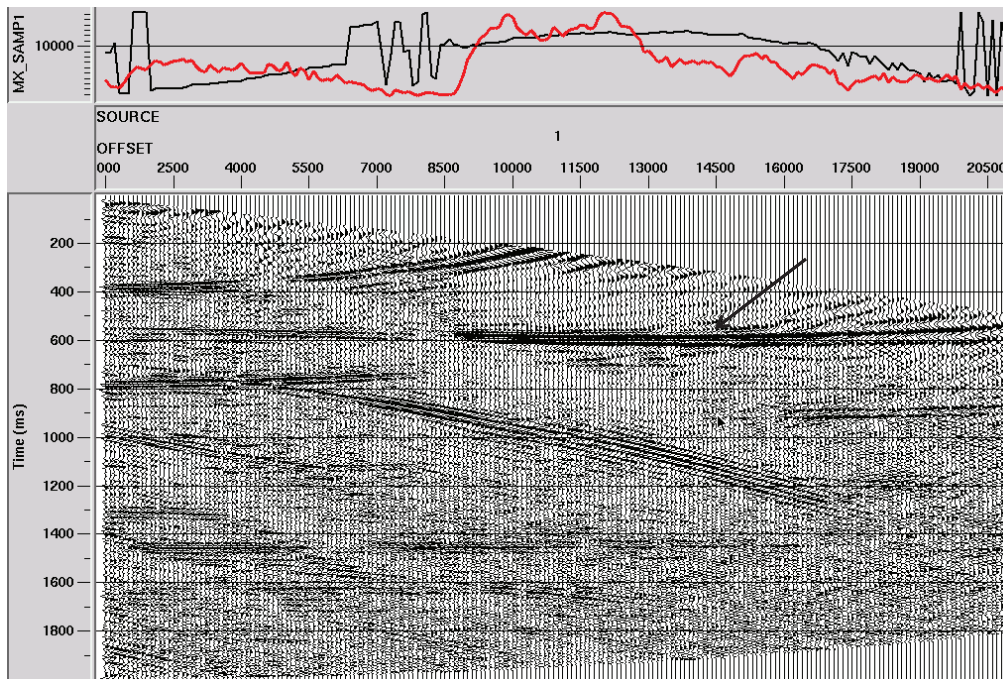
Figures 3, 4, and 5 display the shot gather from Figure 2 after correction for NMO appropriate for selected reflections at 380ms, 550ms, and 750ms, respectively. At the top of each display are two plots, red representing the actual amplitude measurements along the chosen reflection, and black indicating the travel time on each trace at which the amplitude maximum was picked. Black is thus an indicator of the quality of the red amplitude measurement. The more smoothly the black curve follows the NMO-flattened event in time, the more credible the amplitudes. For these fully processed data, the event

at 550ms seems to give the most reliable amplitudes, the main measurement uncertainty occurring where residual noise interferes with the event, or where the event begins to weaken at its longest offset. Both the 380ms and 750ms events terminate at less than the maximum offset, due to stretch muting in the NMO operation for the 380ms event, and weak amplitudes for the 750ms event (which is probably a shear wave, judging from its low NMO velocity and lower amplitudes near zero offset). We used the described amplitude measurement procedure after each significant processing step, for each of the first two reflection events. In the case of the third event, we chose, instead, to analyze the faster overlying event at 775ms because the amplitudes near zero offset are almost certainly those of the 775ms event and not the 750ms event (amplitudes decrease to zero near vertical incidence for shear waves).



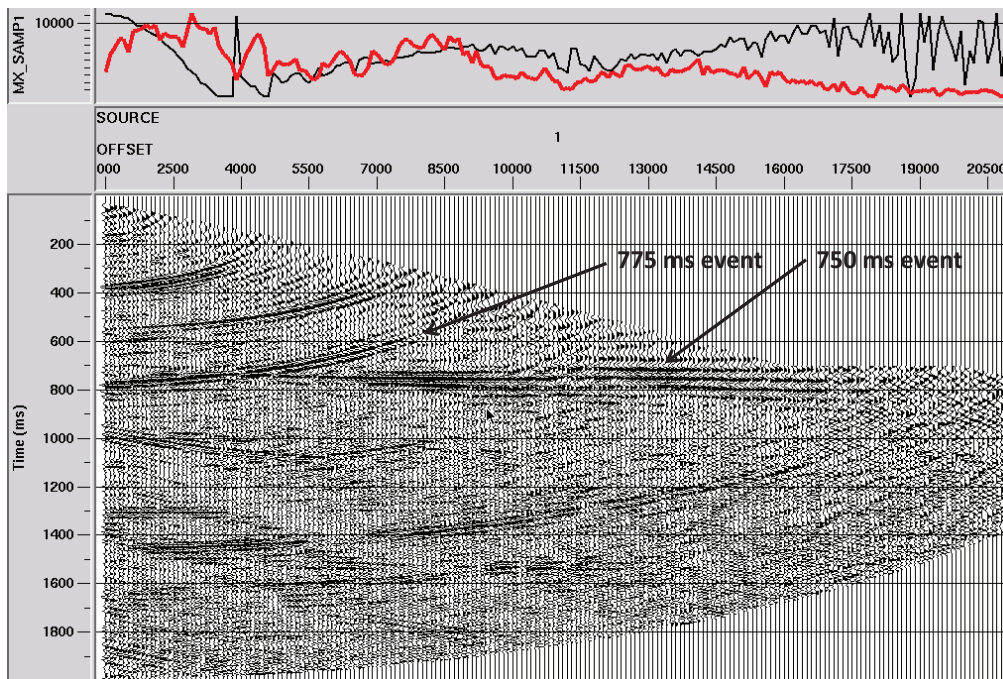
Amplitude analysis of reflection event at 380 ms

FIG. 3. Processed source gather with NMO applied for the event at 380ms. Amplitude analysis was applied along the event. Red=trace amplitude, black=time at which amplitude was measured. Interfering noise obviously causes amplitude mis-picks (black curve deviations).



Amplitude analysis of reflection event at 550 ms

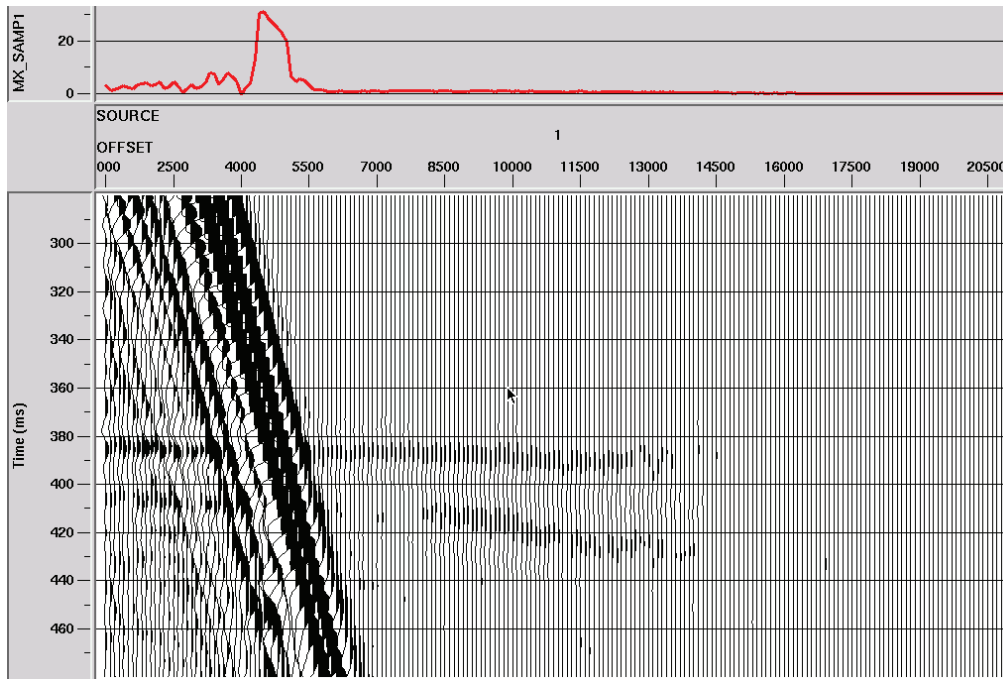
FIG. 4. Processed source gather with NMO applied for the event at 550ms. Amplitude analysis was applied along the event. Red=trace amplitude, black=time at which amplitude was measured. Interfering noise obviously causes amplitude mis-picks (black curve deviations).



Amplitude analysis of reflection event at 750 ms

FIG. 5. Processed source gather with NMO applied for the event at 750ms. Amplitude analysis was applied along the event. Red=trace amplitude, black=time at which amplitude was measured. Note that the 750ms event is the slower of two overlapping events, probably a shear wave event. Amplitudes near zero offset are thus probably those of the 775ms event.

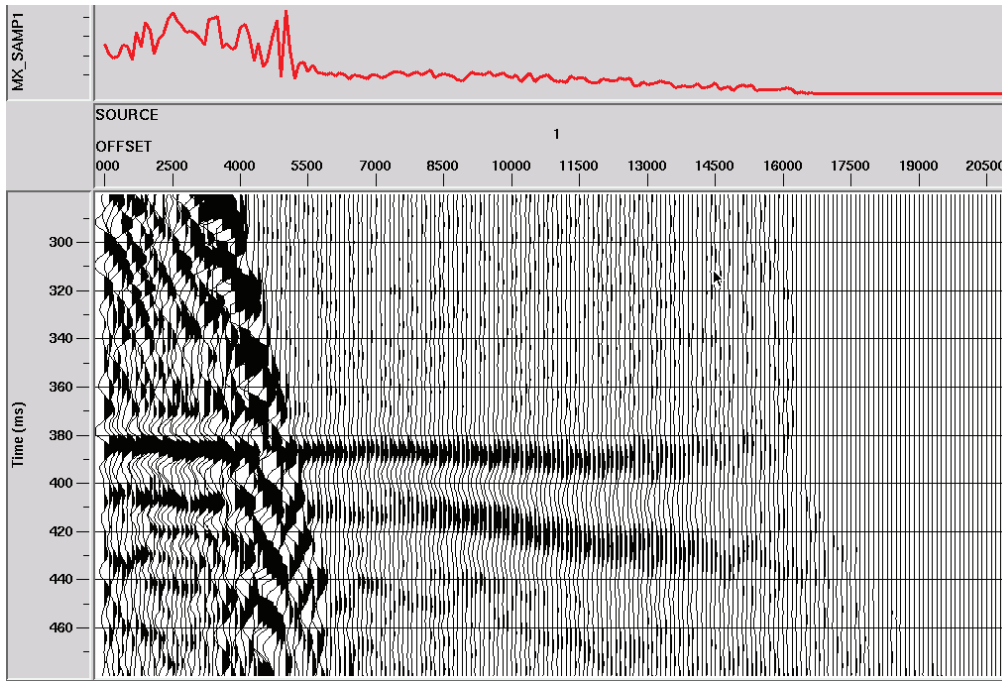
Figure 6 shows the 380ms event as measured on the raw seismic record, with no processing applied except for the NMO correction and noise-limiting bandpass. The amplitude measurements plotted along the top show the strength of the surface wave relative to the very faint reflection amplitudes.



Reflection amplitudes measured along 380 ms event—only NMO and bandpass applied

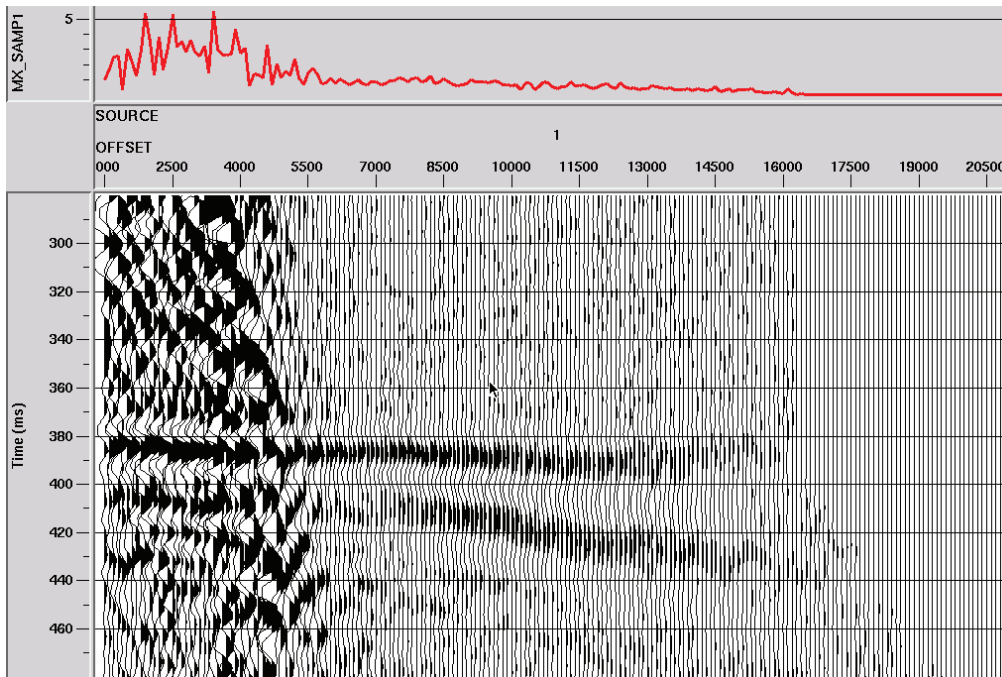
FIG. 6. Amplitude analysis of the reflection event at 380ms. Event was corrected for NMO, then bandpassed to remove high-frequency noise, prior to the amplitude measurements. The red amplitude plot shows that the surface wave amplitudes dominate these measurements.

After estimation and subtraction of the strongest component of the surface wave by radial trace filtering, the analysis is shown in Figure 7. It is obvious on this plot that the interference of the noise with the reflection event has been greatly reduced, and that reflection amplitudes are much larger relative to the noise. Removing more linear coherent energy via several passes of radial trace filtering result in the analysis in Figure 8, in which the overall shape of the reflection amplitude curve changes little from that in Figure 7.



Reflection amplitudes measured along 380 ms event—Surface wave attenuated by radial trace filter, NMO and bandpass applied

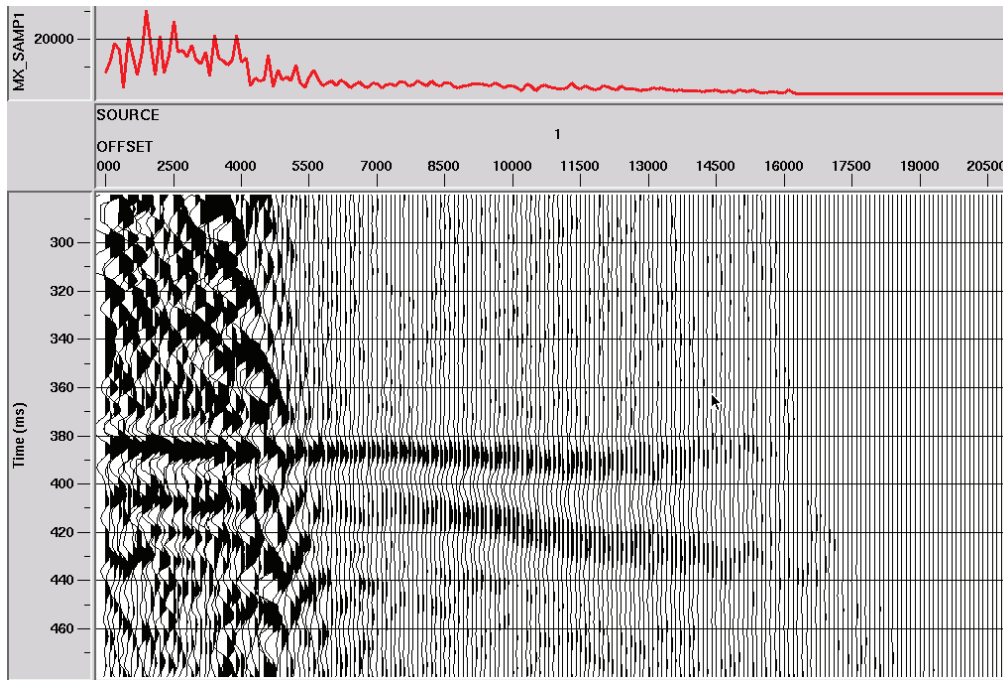
FIG. 7. Amplitude analysis of 380ms reflection event after attenuation of the surface wave by radial trace filtering.



Reflection amplitudes measured along 380 ms event—All visible coherent noise attenuated by radial trace filters, NMO and bandpass applied

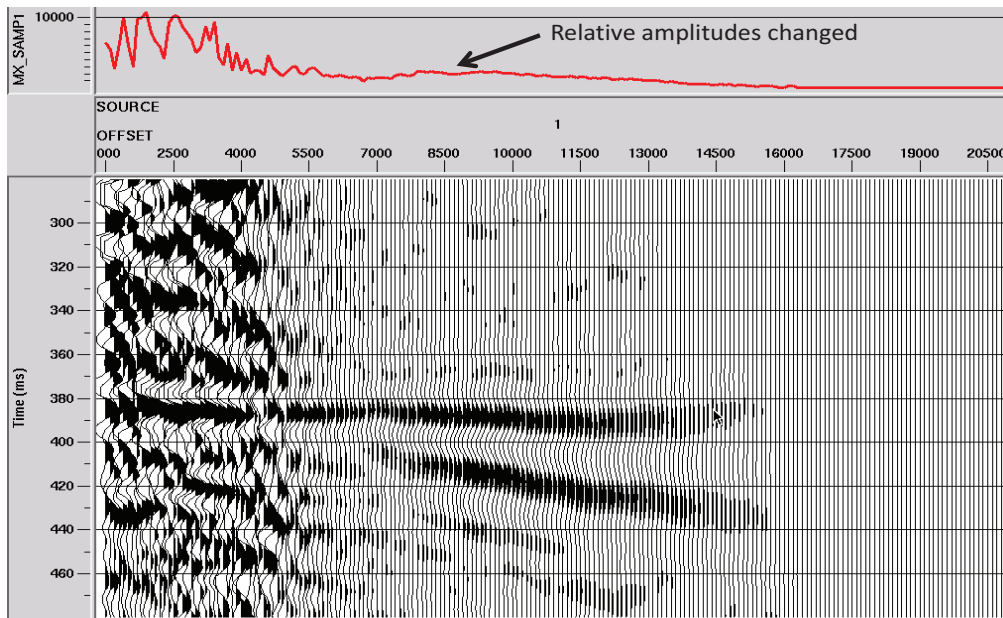
FIG. 8. Amplitude analysis of 380ms reflection event after attenuation of most remaining visible coherent noise by radial trace filtering.

Applying Gabor deconvolution to sharpen the wavelet of the reflection has little visible effect on the the appearance of the reflection or its amplitude curve, as shown in Figure 9. Applying F-X deconvolution to reduce random noise, however, does cause a small but visible change in the shape of the amplitude curve (Figure 10) in the middle of the range of offsets, as well as reducing the jitter in the trace-to-trace amplitudes. Applying a final pass of radial filtering to remove a few residual linear noises causes almost no additional change in the amplitude analysis, as shown in Figure 11. Since it is evident, even at the scale of the plot in Figure 10, that F-X deconvolution alters relative reflection amplitudes, we removed this process and then reapplied the final radial filter pass. The results are shown in Figure 12, where the measured amplitudes for the various stages of processing are plotted at the same scale in the upper part of the figure. In spite of the ‘busy-ness’ of the plot, it can be seen that the slowly varying part of the reflection amplitudes (the part attributable to AVO) coincides for all three analyses for the intermediate and longer offsets and diverges only in the near offsets where the analyses were the most affected by residual coherent noise. The relatively large “jitter” exhibited by all the analyses are attributable primarily to the random noise contaminating this relatively weak event. This could likely be reduced by increasing the vertical stack during data acquisition.



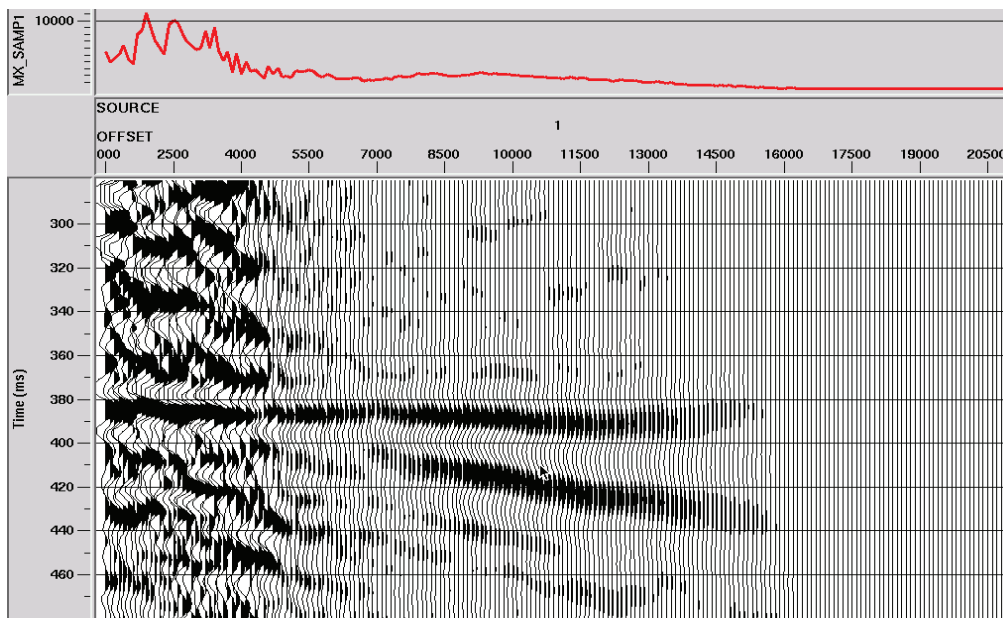
Reflection amplitudes measured along 380 ms event—Coherent noise attenuated by radial trace filters, Gabor deconvolution applied, NMO and bandpass applied

FIG. 9. Amplitude analysis of 380ms reflection event after attenuation of all visible coherent noise and Gabor deconvolution. The deconvolution causes little visible change to the data, and the amplitude measurements are not affected, either.



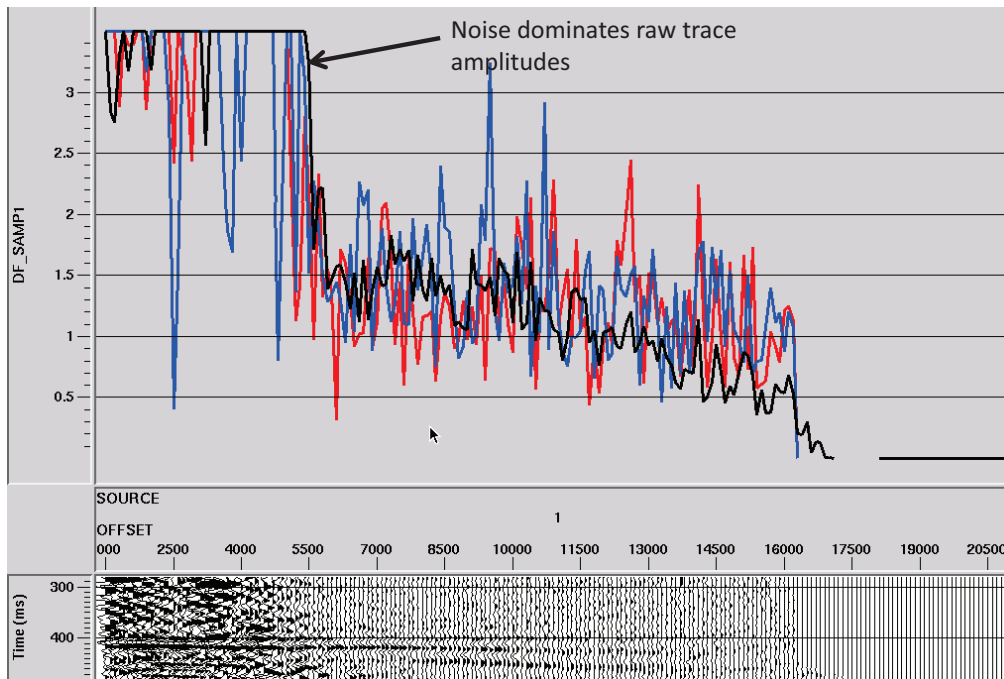
Reflection amplitudes measured along 380 ms event—Coherent noise attenuated by radial trace filters, Gabor deconvolution applied, F-X deconvolution applied, NMO and bandpass applied

FIG. 10. Amplitude analysis of 380ms reflection event after coherent noise attenuation, Gabor deconvolution, and F-X deconvolution. Comparing the red amplitude curves in Figures 9 and 10 shows that the F-X deconvolution alters the apparent AVO relationships along this reflection.



Reflection amplitudes measured along 380 ms event—Coherent noise attenuated by radial trace filters, Gabor deconvolution applied, F-X deconvolution applied, residual linear events attenuated by radial trace filters, NMO and bandpass applied

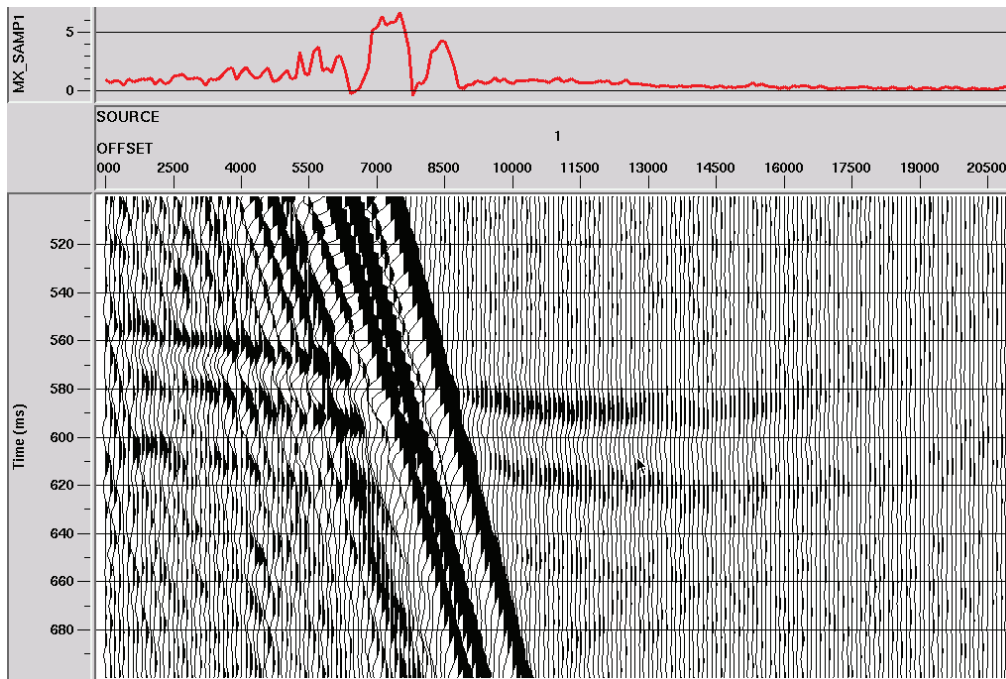
FIG. 11. Amplitude analysis of 380ms reflection event after coherent noise attenuation, Gabor deconvolution, F-X deconvolution, and attenuation of residual linear noise. Only the F-X deconvolution has affected the amplitude curve.



Comparison of amplitude analyses for 380 ms reflection. Black=amplitudes on raw traces; blue=coherent noise attenuated; red=coherent noise attenuated+Gabor deconvolution

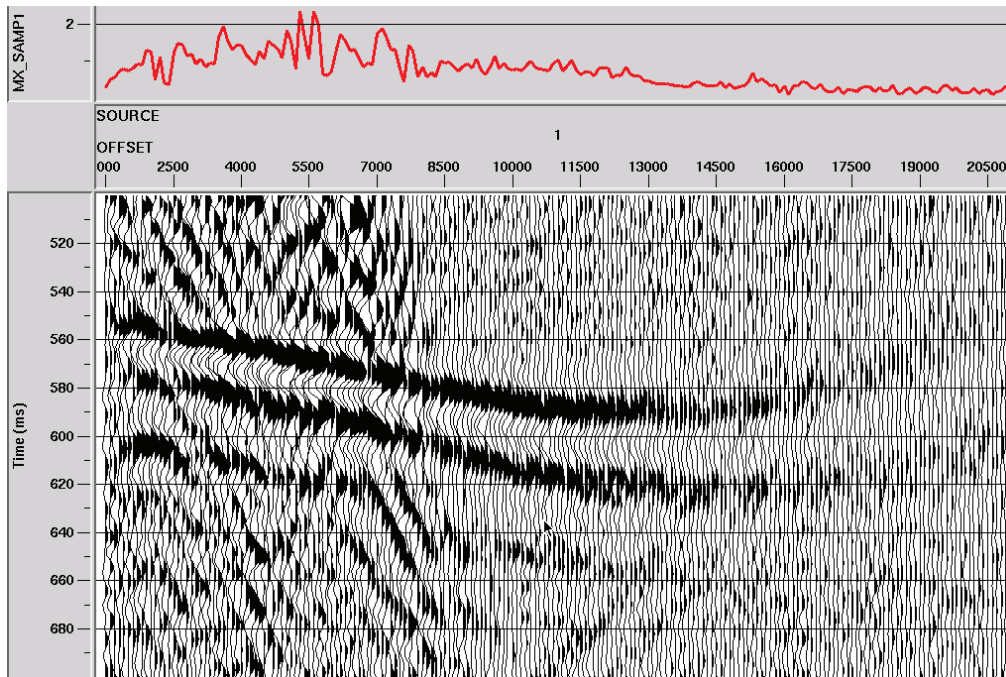
FIG. 12. Comparison of amplitude analyses for 380ms reflection event. The curves are plotted at the same scale. Random fluctuations around the ‘average’ amplitude curves are due to random noise superimposed on the relatively weak reflection, emphasized because of the scale of the plot. Black=raw trace amplitudes; blue=coherent noise attenuated; red=coherent noise attenuated+Gabor deconvolution. Within the jitter of the measurements, the trace-to-trace AVO relationships along this reflection appear to be unaffected by multiple passes of radial trace filtering and a pass of Gabor deconvolution.

Next, we analyzed the stronger reflection at 550 ms, shown in its unprocessed state in Figure 13. As with the shallower event, the amplitude analysis for this reflection is dominated by the surface wave. When this energy is removed by radial trace filtering, the analysis is as shown in Figure 14. After removal of more linear noise, Figure 15 shows the resulting analysis, which differs little from Figure 14. Likewise, Gabor deconvolution has no appreciable effect on the analysis (Figure 16), but F-X deconvolution appears to alter the underlying curve shape in the mid-range of offsets (Figure 17). Figure 18 shows, once again, the result of omitting the F-X deconvolution and adding another radial filter pass to remove some residual linear noise. The analysis overlay plot in Figure 19 confirms that the underlying AVO relationships appear to remain undisturbed by the passes of radial trace filtering and Gabor deconvolution. We also see on Figure 19 that the amplitude fluctuations from trace to trace are less than those for the shallower event. This is almost certainly due to the fact that the reflection is stronger relative to the contaminating random noise than the 380 ms reflection. Comparing the event plots in both Figures 12 and 19 seems to confirm that judgement.



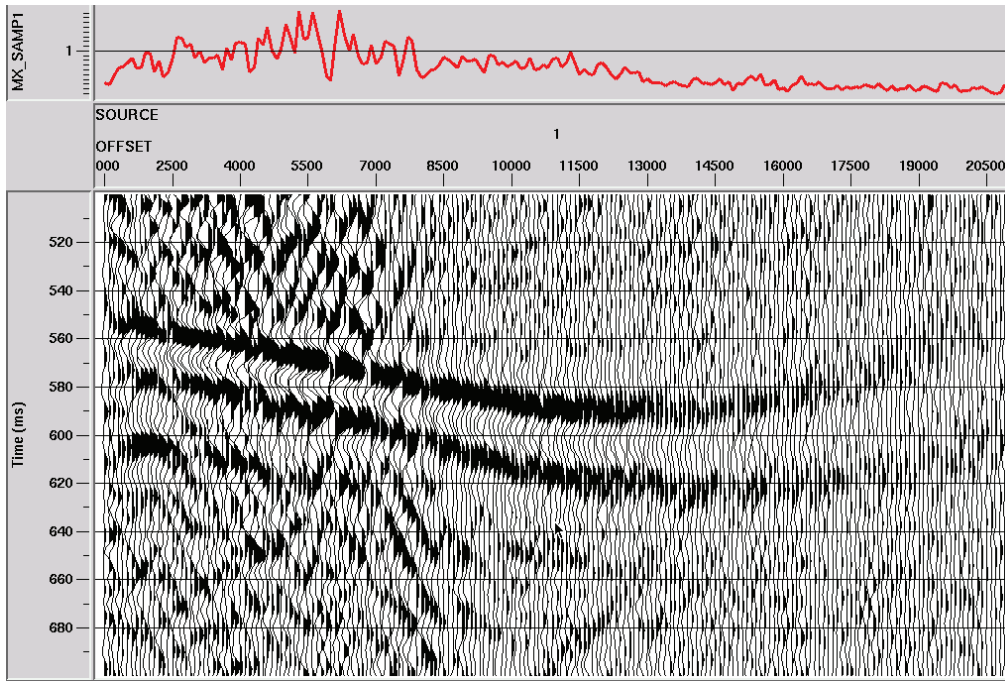
Reflection amplitudes measured along 550 ms event—only NMO and bandpass applied

FIG. 13. Amplitude analysis of the reflection event at 550ms. Event was corrected for NMO, bandpassed to remove high-frequency noise before amplitudes were measured. The surface wave amplitudes dominate the amplitude curve for these unprocessed data.



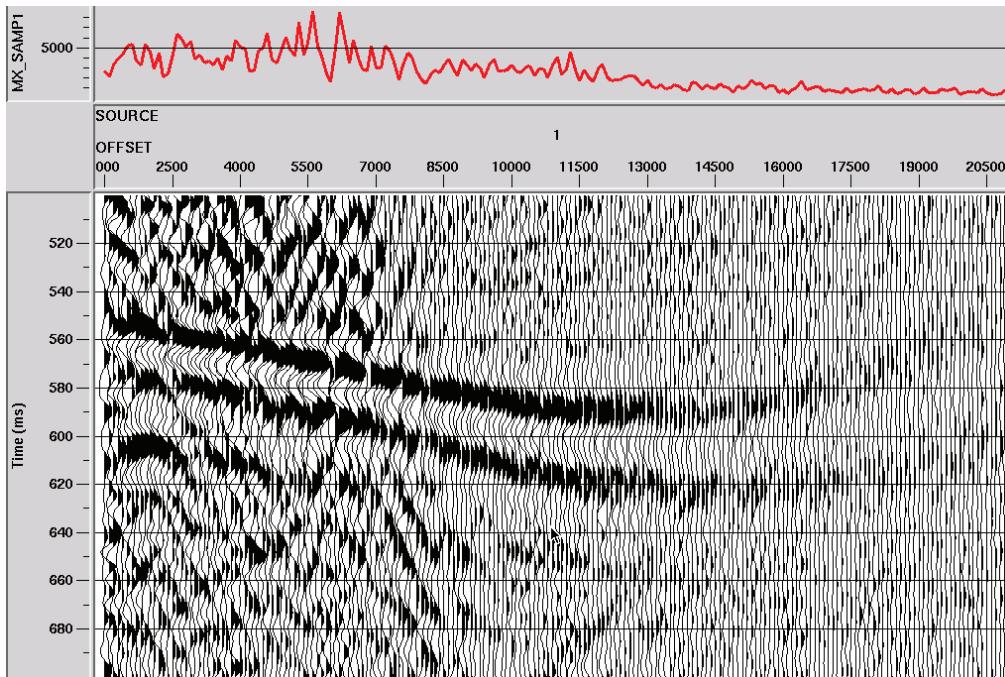
Reflection amplitudes measured along 550 ms event—Surface wave attenuated by radial trace filter, NMO and bandpass applied

FIG. 14. Amplitude analysis of the 550ms reflection event after attenuation of the surface wave by radial trace filtering.



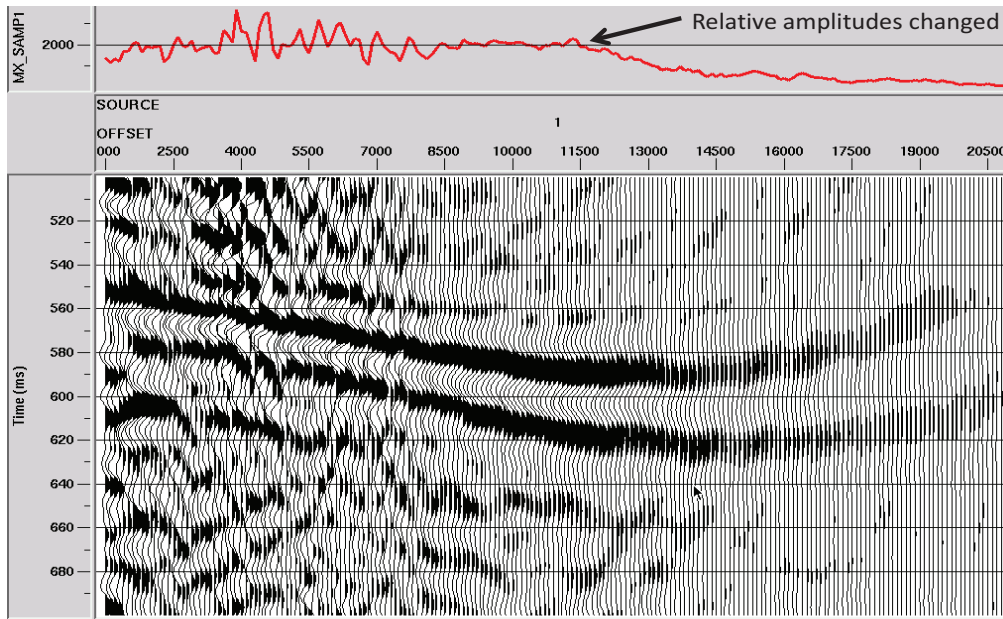
Reflection amplitudes measured along 550 ms event—All visible coherent noise attenuated by radial trace filters, NMO and bandpass applied

FIG. 15. Amplitude analysis of the 550ms reflection event after coherent noise attenuated by radial trace filtering.



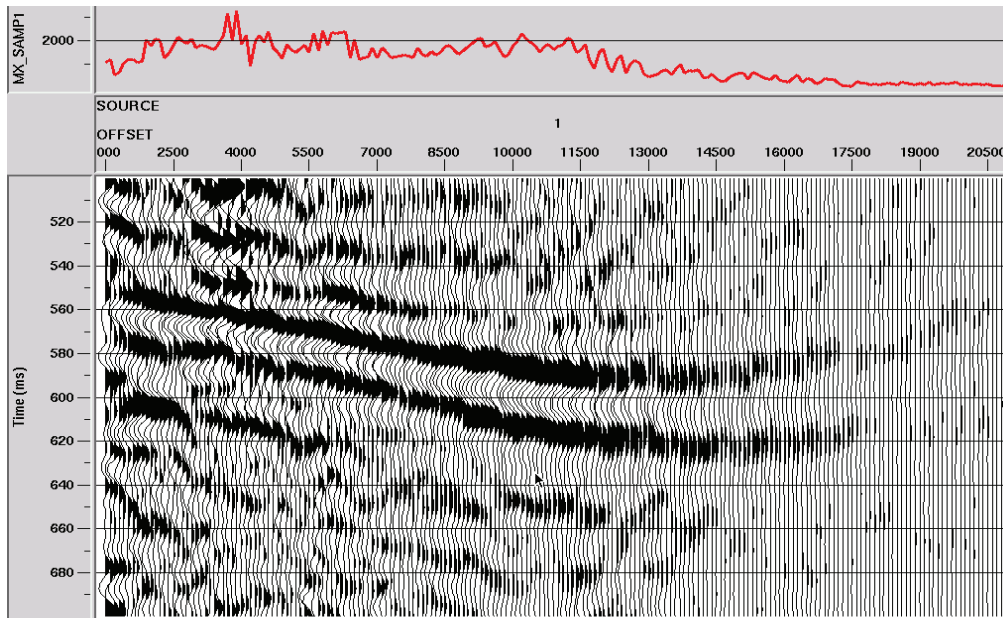
Reflection amplitudes measured along 550 ms event—Coherent noise attenuated by radial trace filters, Gabor deconvolution applied, NMO and bandpass applied

FIG. 16. Amplitude analysis of the 550ms reflection event after coherent noise attenuation and Gabor deconvolution. Deconvolution has little effect on the reflection, or its amplitudes.



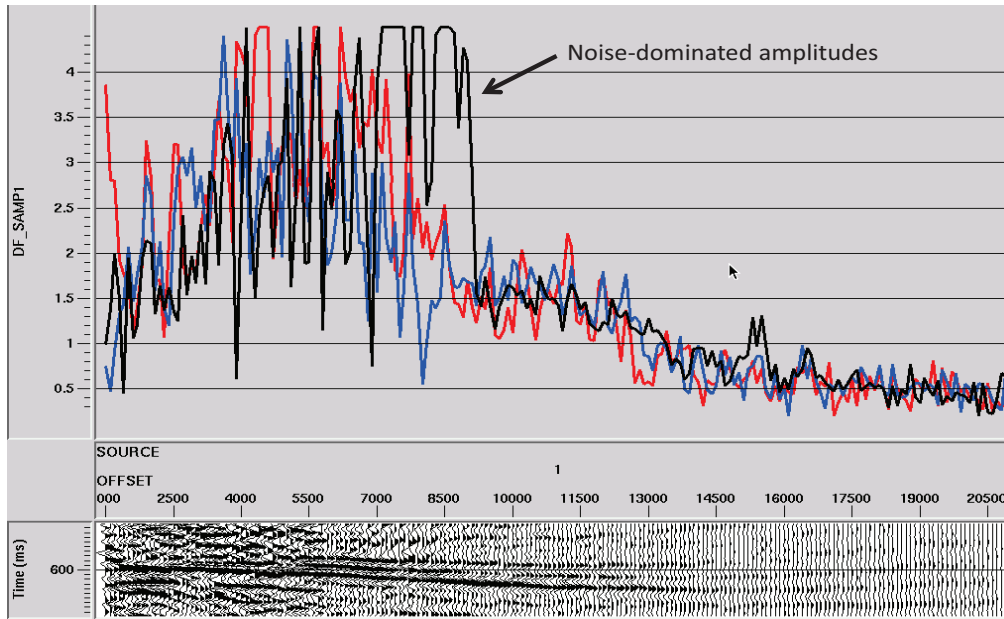
Reflection amplitudes measured along 550 ms event—Coherent noise attenuated by radial trace filters, Gabor deconvolution applied, F-X deconvolution applied, NMO and bandpass applied

FIG. 17. Amplitude analysis of the 550ms reflection event after coherent noise attenuation, Gabor deconvolution, and F-X deconvolution. The effect of the F-X deconvolution on the amplitude curve in its mid-range offsets can be seen by comparing with Figure 16.



Reflection amplitudes measured along 550 ms event—Coherent noise attenuated by radial trace filters, Gabor deconvolution applied, F-X deconvolution applied, residual linear events attenuated by radial trace filters, NMO and bandpass applied

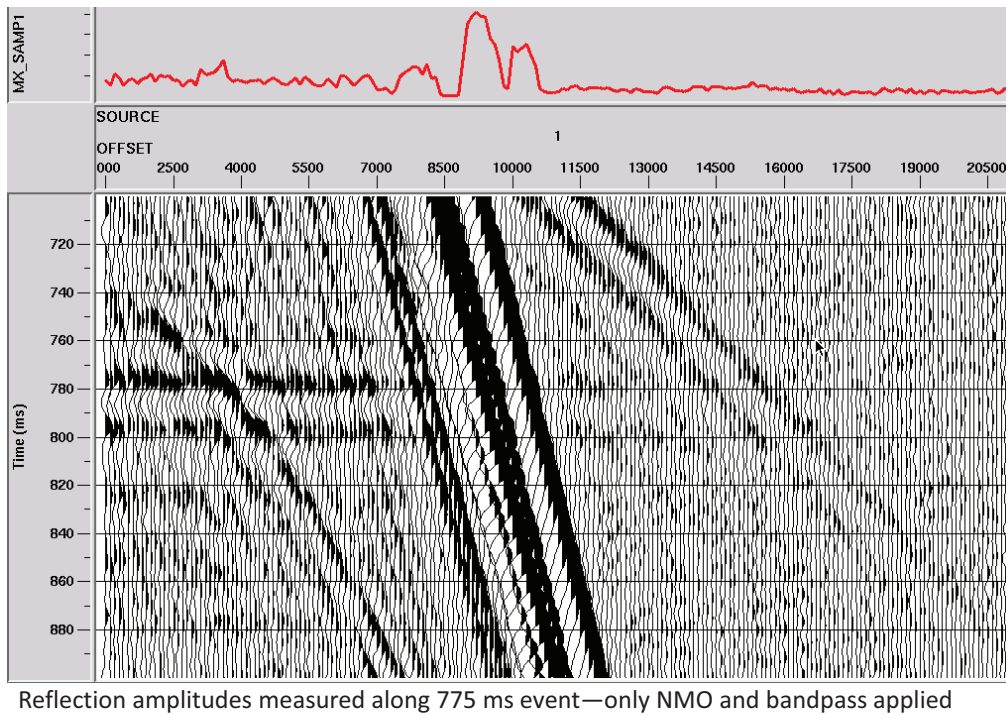
FIG. 18. Amplitude analysis of the 550ms reflection event after coherent noise attenuation, Gabor deconvolution, F-X deconvolution, and attenuation of residual linear events. The largest effect on AVO relationships is due to the F-X deconvolution.



Comparison of amplitude analyses for 550 ms reflection. Black=amplitudes on raw traces; red=coherent noise attenuated; blue=coherent noise attenuated+Gabor deconvolution

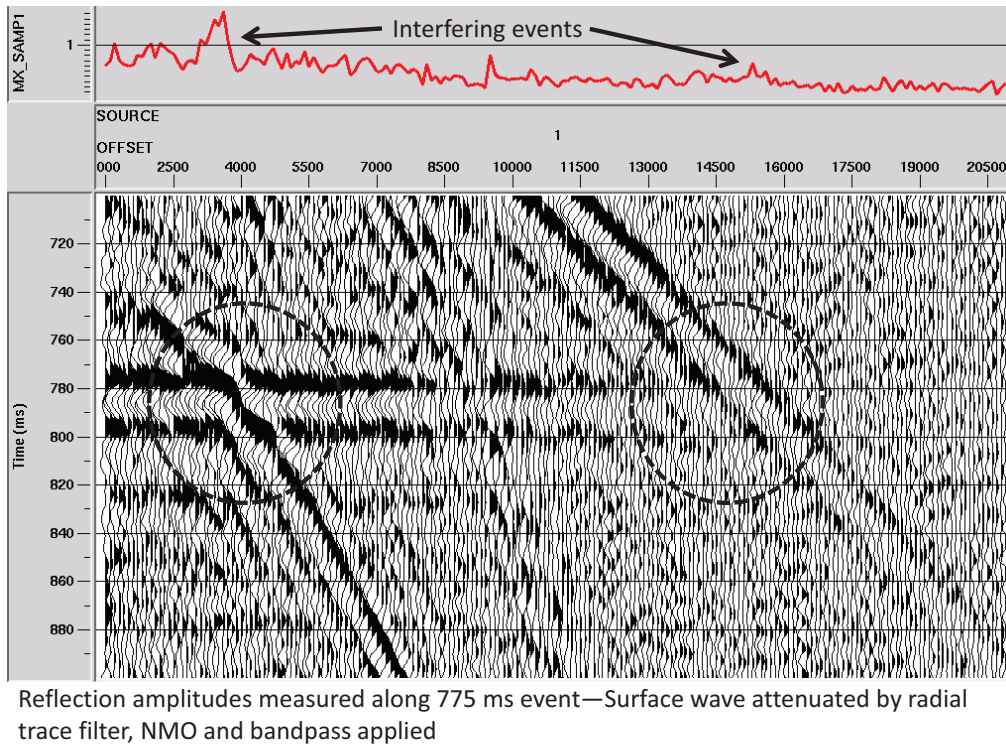
FIG. 19. Comparison of amplitude curves for the 550ms reflection event. Since this event is much stronger than the 380ms event, the superimposed random noise contributes to much smaller jitter in the amplitude curves for this event. Black=unprocessed traces; red=coherent noise attenuated by radial filtering; blue=coherent noise attenuated+Gabor deconvolution. The radial trace filtering and Gabor deconvolution do not alter the AVO relationships along this reflection event.

Rather than analyze the 750 ms event shown in Figure 5, we chose to analyze the interfering event at 775 ms, which overlies the 750 ms event, has higher NMO velocity, and amplitudes that decrease with offset. Figure 20 shows this event and its amplitude analysis. The event is not even visible at the farthest offsets, and over much of the mid-range of offsets, it is obscured by surface wave noise. After the surface wave event is removed, we can still see two interfering hyperbolic events whose presence can be clearly seen on the amplitude plot in Figure 21. Removing more linear noise results in Figure 22, whose amplitude analysis differs little from Figure 21. Gabor deconvolution has little effect on amplitudes (Figure 23), but F-X deconvolution visibly effects amplitudes in Figure 24. Removing the limbs of the interfering hyperbolic events via radial trace filtering makes the reflection amplitude variation with amplitude smoother, and also makes the reflection visible (barely) all the way to the farthest offsets (Figure 25). The overlay amplitude analysis plot in Figure 26 confirms that even for this reflection with very weak amplitudes at long offsets, the AVO trends within the amplitude analysis windows remain intact after multiple passes of radial trace filtering and Gabor deconvolution.



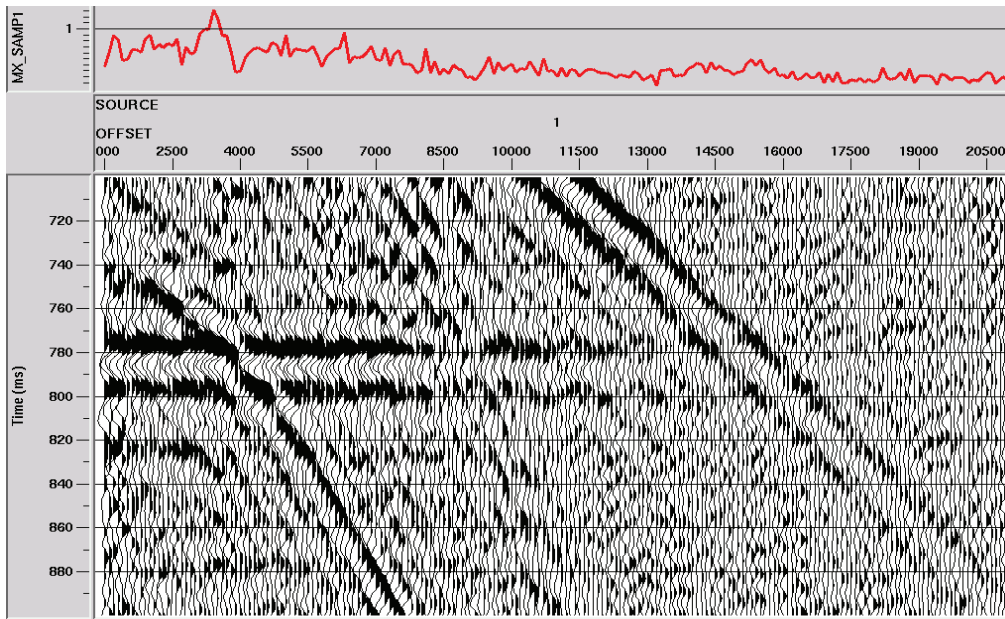
Reflection amplitudes measured along 775 ms event—only NMO and bandpass applied

FIG. 20. Amplitude analysis of the fast reflection event at 775ms. As with the other two events chosen for analysis, the surface wave dominates the amplitude curve.



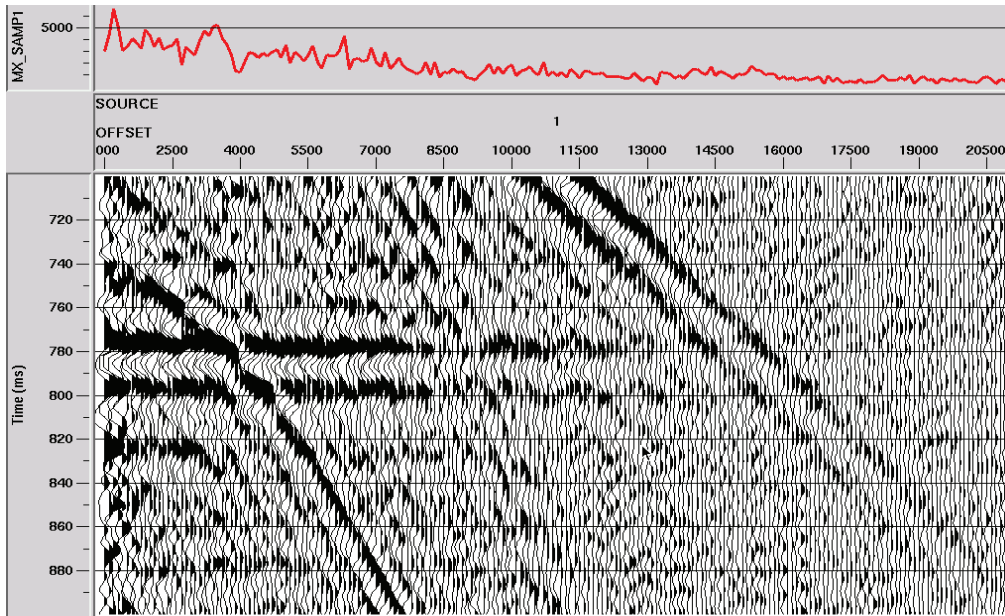
Reflection amplitudes measured along 775 ms event—Surface wave attenuated by radial trace filter, NMO and bandpass applied

FIG. 21. Amplitude analysis of the 775ms reflection event after attenuation of the surface wave by radial trace filtering. The amplitude curve now shows mainly the effects of two other interfering events.



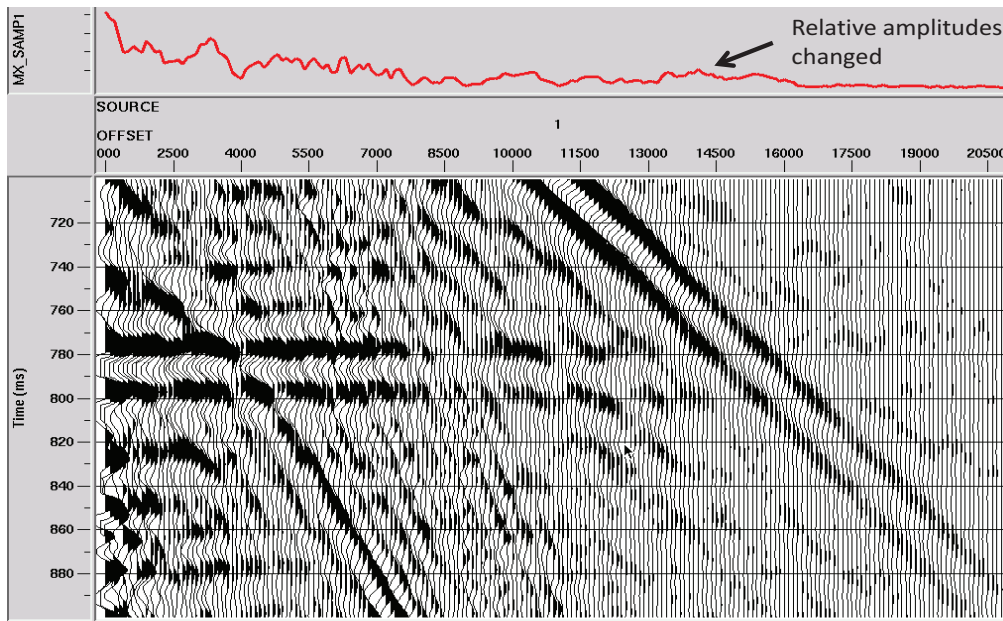
Reflection amplitudes measured along 775 ms event—All visible coherent noise attenuated by radial trace filters, NMO and bandpass applied

FIG. 22. Amplitude analysis of the 775ms reflection event after most visible linear noise attenuated by radial trace filtering (interfering events are non-linear and weren't targeted at this stage).



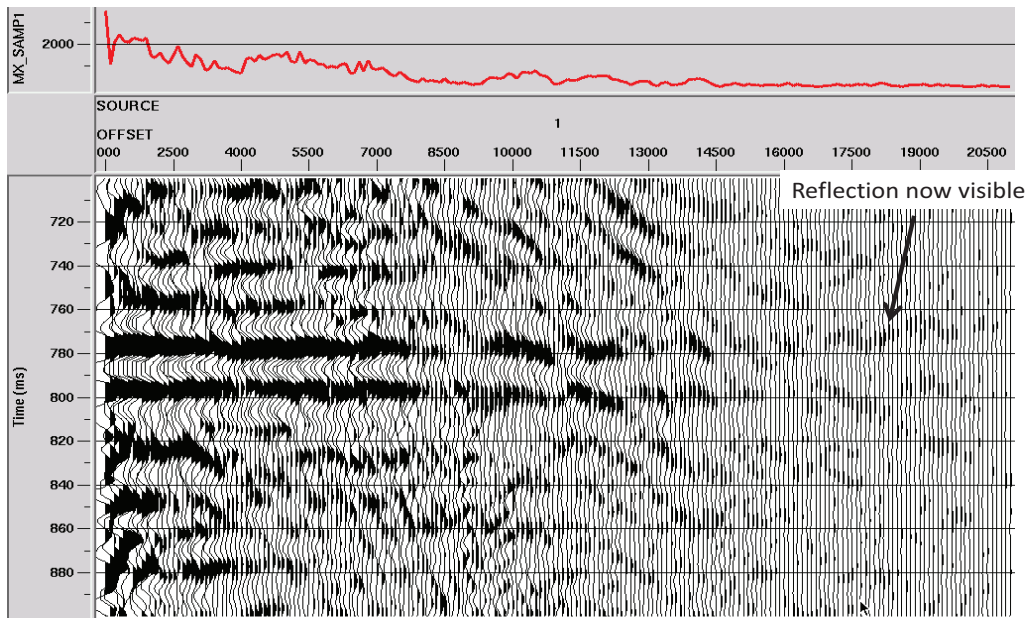
Reflection amplitudes measured along 775 ms event—Coherent noise attenuated by radial trace filters, Gabor deconvolution applied, NMO and bandpass applied

FIG. 23. Amplitude analysis of the 775ms reflection event after coherent noise attenuation and Gabor deconvolution. The deconvolution has little effect on event appearance or the amplitude curve.



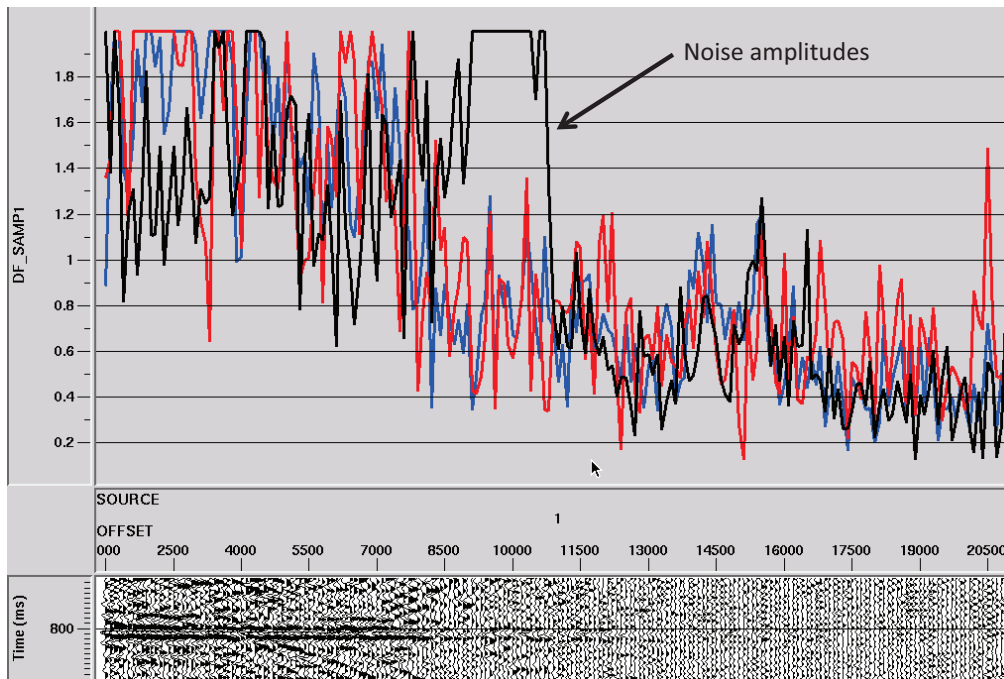
Reflection amplitudes measured along 775 ms event—Coherent noise attenuated by radial trace filters, Gabor deconvolution applied, F-X deconvolution applied, NMO and bandpass applied

FIG. 24. Amplitude analysis of the 775ms reflection event after coherent noise attenuation, Gabor deconvolution, and F-X deconvolution. The F-X deconvolution is the only operation that affects the shape of the amplitude curve in the mid-range offsets.



Reflection amplitudes measured along 775ms event—Coherent noise attenuated by radial trace filters, Gabor deconvolution applied, F-X deconvolution applied, residual linear events attenuated by radial trace filters, NMO and bandpass applied

FIG. 25. Amplitude analysis of the 775ms reflection event after coherent noise attenuation, Gabor deconvolution, F-X deconvolution, and residual coherent noise attenuation. Only the F-X deconvolution has affected the shape of the amplitude curve in the mid-range offsets. The reflection is now barely visible at the longer offsets.



Comparison of amplitude analyses for 775 ms reflection. Black=amplitudes on raw traces; red=coherent noise attenuated; blue=coherent noise attenuated+Gabor deconvolution

FIG. 26. Comparison of the amplitude analyses for the 775ms reflection event. Since this event is weaker, superimposed random noise leads to larger jitter in the amplitude measurements than for the 550ms reflection. The underlying AVO relationship appears to be the same for all three analyses, however. Black=unprocessed trace amplitudes; red=coherent noise attenuated by radial filtering; blue=coherent noise attenuated+Gabor deconvolution.

DISCUSSION

The results presented appear to confirm our earlier conjectures about the effects of various processing operations on the trace-to-trace amplitudes of seismic reflections. Subtracting coherent noise estimates derived in the radial trace domain seems to have no significant effect on AVO amplitude relationships, except for the traces which are originally overlaid by the noise. If the parameters for the noise estimation allow reflection energy to leak into the noise estimate, however, then we would expect that AVO relationships could possibly change, since energy is subtracted from the reflection as well as the noise. As expected, non-stationary deconvolution applied to single traces independently had no discernable effect on reflection amplitude relationships, but a process like F-X deconvolution which predicts amplitudes across traces does affect AVO relationships and should probably be avoided when these relationships need to be preserved, unless the random noise level is so high that trace-to-trace amplitude jitter needs to be reduced significantly.

Although not discussed earlier, or analyzed for amplitude preservation, there is another radial trace domain operation that can affect AVO relationships: normalization in the R-T domain (Henley, 2011). This operation is used to reduce the amplitude of a very strong linear event with respect to background reflections. When whole trace normalization is applied in the R-T domain, the operation will damage AVO relationships

to some extent. In the worst case, if a short window AGC is applied in the R-T domain, the AVO relationships of the original data will be destroyed.

CONCLUSIONS

Preserving trace-to-trace amplitude relationships is important for using reflection or conversion AVO as a diagnostic tool for lithologic information and rock fluid content. In light of this, when we process raw data to make them interpretable, we must be aware of the potential effects of the processing on the underlying AVO relationships. In this empirical study, we have analyzed three different reflection events on a trace gather from a physical model experiment. Our analysis confirms our initial intuition about which processing operations disturb AVO relationships and which do not. Single-trace operations appear not to be a concern, in general, as long as they are properly normalized, and as long as they don't normalize a trace ensemble to a common level. Multi-trace operations, on the other hand, generally alter relative event amplitudes. An exception to this is a process like radial trace filtering, which makes multi-trace estimates of noise and subtracts the noise. As long as the noise estimate contains no reflection energy, the AVO relationships of reflections will not be disturbed. R-T domain normalization and AGC, however, irreversibly alter AVO relationships.

ACKNOWLEDGEMENTS

The authors thank the sponsors of CREWES for ongoing support.

REFERENCES

- Henley, D.C., 2003, Coherent noise attenuation in the radial trace domain, *Geophysics*, **68**, No. 4, pp1408-1416.
- Henley, D.C., 2003, More coherent noise attenuation in the radial trace domain, CREWES Research Report, **15**.
- Henley, D.C., 2011, Now you see it, now you don't: radial trace filtering tutorial, CREWES Research Report, **23**.
- Margrave, G.F., and Lamoureux, M.P., 2002, Gabor deconvolution: 2002 CSEG Annual Convention, Expanded abstracts.
- Margrave, G.F., Linping Dong, Grossman, J.P., Henley, D.C., and Lamoureux, M.P., 2003, Gabor deconvolution: extending Wiener's method to nonstationarity: CREWES Research Report, **15**.
- Wong, J., Hall, K.W., Bland, H.C., Gallant, E.V., and Bertram, M.B., 2007, Some 2D results from the U of C Seismic Physical Modelling Facility, CREWES Research Report, **19**.
- Wong, J., Hall, K.W., Gallant, E.V., and Bertram, M.B., 2008, Mechanical and electronic design for the U of C Seismic Physical Modelling Facility, CREWES Research Report, **20**.
- Wong, J., Hall, K.H., Gallant, E.V., Maier, R., Bertram, M.B., and Lawton, D.C., 2009. Seismic physical modeling at the University of Calgary: CSEG Recorder, **34**, pp 36-43.